

SHTC2024-121704

3D PRINTED CAPILLARY-DRIVEN COLD PLATE FOR HYBRID TWO-PHASE COOLING SYSTEM

Mohammad Reza Shaeri, Maksym Demydovych
Advanced Cooling Technologies, Inc., Lancaster, PA, 17601, USA

ABSTRACT

In this study, a hybrid two-phase cooling system (HTPCS) was developed for thermal management of high-heat-flux electronics. The HTPCS integrates capillary-driven evaporation from wicks with mechanically pumped two-phase cooling. The capillary-driven evaporation takes place within a compact cold plate housing eight heaters situated on both sides of the cold plate, each heater dedicated to an individual evaporator wick. The significance of this study lies in fabricating the entire cold plate through one single 3D printing process. Constructed from AlSi10Mg using a Direct Metal Laser Sintering process, the cold plate operated with the refrigerant R245fa across a broad range of heat fluxes. Comparative analysis was performed with a 3D printed plain cold plate (i.e., without evaporator wicks). The HTPCS demonstrated stable operation at heat fluxes exceeding 305 W/cm^2 , marking a more than 103% improvement in the upper limit operation compared to the plain cold plate. Within this heat flux range, the measured thermal resistances achieved by the HTPCS were ~ 0.17 to $0.24 \text{ K-cm}^2/\text{W}$. The developed HTPCS emerges as a promising solution for thermal management in high-heat-flux applications. Furthermore, the fact that the fabrication process for the cold plate involves only one 3D printing step significantly streamlines the commercialization of the HTPCS developed in this study.

Keywords: Thermal management; Hybrid two-phase cooling; Capillary-driven evaporation; Evaporator wicks; 3D printing.

1. INTRODUCTION

The rapid reduction in size of electronic components has presented an unprecedented challenge in effective thermal management of these miniaturized devices, given the continuously rising heat flux [1–3]. Removing high heat fluxes that exceed 1 kW/cm^2 over small-sized footprint areas [4,5] is not only beyond the capacity of air and single-phase liquid cooling systems [6], but it also surpasses the capability of high-

performance two-phase cooling systems [7]. The utilization of capillary-driven evaporation from wick structures has been recognized as an efficient cooling method for dissipating significant amounts of heat without relying on external power sources. However, the upper limit of operation for a capillary-driven two-phase system, like a heat pipe, is constrained by the capillary pressure generated by the wick [8]. While pumped two-phase cooling systems such as micro/minichannel heat sinks overcome this limitation and allow the heat to be transported over a long distance, they are prone to the limitations of flow boiling instabilities that can accelerate the occurrence of critical heat flux (CHF) [9,10].

To overcome the limitations of individual two-phase cooling technologies, Shaeri et al. [11] developed a hybrid two-phase cooling system (HTPCS) that integrated capillary-driven evaporation from wicks and mechanically pumped two-phase cooling. In this method, heat was extracted from multiple heat sources on the cold plate through capillary-driven evaporation from wick structures. Simultaneously, a mechanical pump continuously supplied the cold plate with liquid coolant. However, despite the significant improvements in thermal performance achieved by the HTPCS in [11], the commercialization of this technology requires further efforts, primarily in the design of the cold plate. The cold plates in [11] was fabricated through several labor-intensive steps including CNC machining of the cold plate components, a high-temperature sintering process for creating evaporator wicks, and a bonding process to assemble the cold plate. All of these processes are costly and time-consuming, which hinders the commercialization of the developed HTPCS.

The objective of this study is to overcome the manufacturing limitations of current versions of cold plates for HTPCS through additive manufacturing (AM), known as 3D printing as well. AM stands as a key enabling technology for creating parts by depositing materials layer-by-layer directly from a CAD model [12–14]. The layer-by-layer fabrication provides substantial

flexibility in producing intricately designed parts with a high level of precision, a capability that traditional manufacturing processes cannot easily match [15,16]. In this study, a cold plate comprising multiple evaporator wicks associated with multiple heat sources was manufactured using one single 3D printing process. The cold plate was tested over a wide range of heat fluxes, and the results were compared to a plain cold plate serving as the reference baseline. The fabrication approach employed in this work condenses the various labor-intensive fabrication processes involved in manufacturing current versions of cold plates for HTPCS into only one 3D printing process. This marks an essential step toward the commercialization of the developed HTPCS in [11]. The present study is a supplement to our previous work in [17,18] aimed at the development of a 3D printed capillary-driven cold plate.

2. EXPERIMENT

In this study, a HTPCS was developed, incorporating a capillary-driven cold plate and a pumped two-phase loop operating with the refrigerant R245fa.

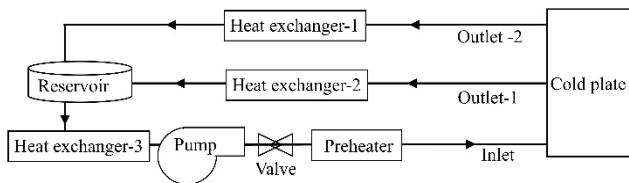


FIGURE 1: SCHEMATIC OF THE DEVELOPED HTPCS

Fig. 1 illustrates the schematic of the developed HTPCS, which consists of a cold plate, a reservoir, several heat exchangers that acted like condensers, and a positive displacement pump. Additionally, a water-cooling loop (not shown in the figure) was fabricated to exchange the heat rejected from the vapor and the two-phase refrigerant in the heat exchangers with lower-temperature water provided by a chiller. At various points along the refrigerant and water loops, such as the inlet and outlet of the cold plate and heat exchangers, Resistance Temperature Detectors (RTDs), pressure transducers, and flowmeters were integrated to measure the flow temperature, flow pressure, and flow rates, respectively. All components of the loop were interconnected using stainless steel tubes.

The CAD model of the cold plate and evaporator wicks are illustrated through Fig. 2 to Fig. 4. The cold plate comprised eight pedestals designed to hold eight heaters. Each heater was associated with an evaporator wick, which was a rectangular porous structure with a thickness of 1 mm. Each pedestal was aligned with the center of its corresponding evaporator. The initial design of the cold plate was intended for thermal management of electronics with a footprint area nearly identical to the small area of the pedestal. However, due to the unavailability of off-the-shelf high-power heaters with the same footprint size, converging pedestals were designed to locate the heaters on the larger area of the pedestal. Due to the initial design requirements of the present HTPCS, the inlet and outlet manifolds were originally situated on the same side, and the cold

plate was equipped with two outlets. However, there are no restrictions on the number of inlet and outlet manifolds, nor their locations on the cold plate.

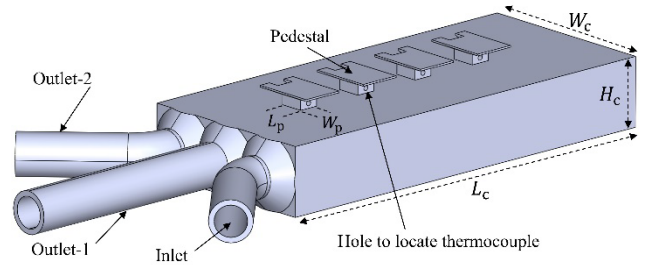


FIGURE 2: CAD MODEL OF THE COLD PLATE

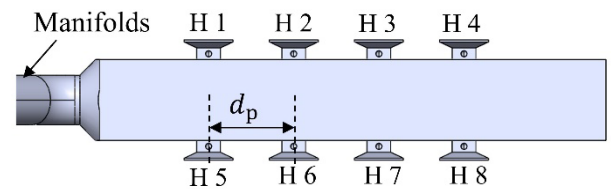


FIGURE 3: SIDEVIEW OF THE COLD PLATE. THE ORDER OF HEATERS ON THE COLD PLATE IS SPECIFIED

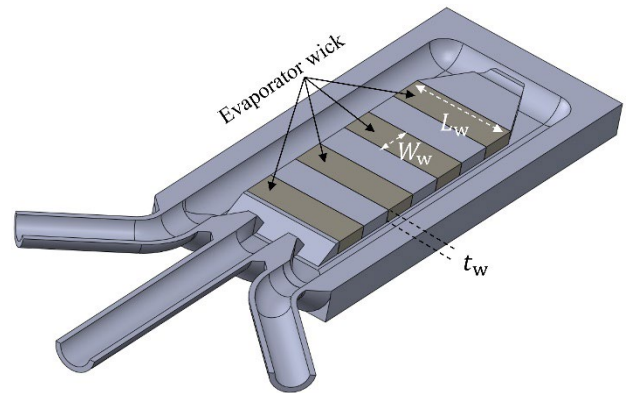


FIGURE 4: CAD MODEL REPRESENTING THE INSIDE OF THE COLD PLATE

Each pedestal featured a hole extending to its midpoint, accommodating a T-type thermocouple for measuring the source temperature (T_s), with the space filled with thermal grease. Electric heat was applied to each pedestal through a resistive heater. On the larger footprint area of each pedestal, a high frequency/RF resistor with a power rating of up to 200 W was mounted using a thermal interface material. To ensure sustained contact between each heater and its corresponding pedestal throughout the experiment, a heater holder unit was fabricated. This unit incorporates eight screws facilitating the insertion of individual heaters into their corresponding pedestals, ensuring

continuous contact. A variable transformer supplied the current and voltage to each individual heater.

Fig. 5 shows the 3D printed cold plate in this study. Two distinct cold plates made of AlSi10Mg were manufactured for this study. The primary cold plate, central to this work, is the capillary-driven cold plate. The second cold plate, referred to as the plain cold plate, featured bare surfaces without evaporator wicks, serving as the baseline for comparison. Both cold plates shared identical dimensions, operated within the same pumped two-phase loop, and were fabricated through one single 3D printing process using Direct Metal Laser Sintering (DMLS) technology. Fabrication of the cold plates and evaporator wicks involved adjusting several build parameters such as laser power, exposure time, hatch distance, point distance, and layer thickness. An in-house methanol bath was made, and the cold plates underwent a continuous methanol flush to eliminate any residual powder that remained inside the cold plate.

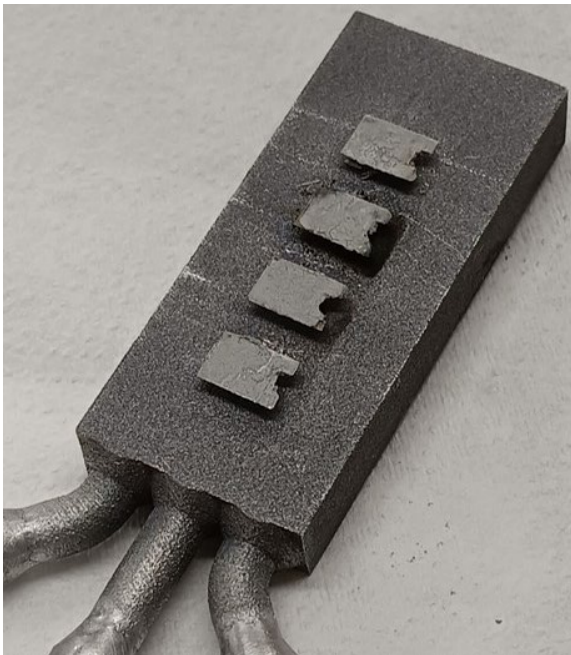


FIGURE 5: 3D PRINTED COLD PLATE IN THIS WORK

Various 3D printed components were also produced to illustrate the internal elements of the cold plate. In Fig. 6, a cross-sectional perspective is presented, highlighting the evaporator wicks (i.e., porous structures). The SEM micrograph representing the evaporator wick is shown in Fig. 7. Table 1 provides the geometrical information for both the cold plate and the evaporator wicks. The hermeticity of the cold plates was confirmed using a helium mass spectrometer, indicating a measured leak rate lower than 9×10^{-10} Std. cc/s [19,20]. Then, the cold plate was inserted into the loop, with the arrangement of heaters shown in Fig. 3, where heaters 1 to 4 were positioned at the top and heaters 5 to 8 were placed on the bottom surface of the cold plate. Prior to conducting the experiment, an examination of the entire loop was carried out to identify any

leaks before charging it with R245fa refrigerant. By adjusting the voltage of the variable transformer, the electrical heat input to an individual heater was elevated. The cold plate was continuously supplied with liquid R245fa at a flow rate of 1.0 LPM (liters per minute) using a mechanical pump. A portion of this liquid was wicked through the evaporator wicks and used for evaporation. The vapor generated from evaporation within the wicks and boiling on the bare surface of the cold plate exited through two outlet manifolds and returned to their respective condensers. The outflows from both condensers were combined within the liquid reservoir. To prevent cavitation in the pump, a heat exchanger, functioning like a condenser, was implemented after the reservoir to ensure that the incoming flow to the pump remained in a single-phase liquid state. Subsequently, the subcooled liquid was pumped into the cold plate, completing the loop. Once a steady-state condition was achieved in the system, characterized by minimal fluctuations in the temperatures measured by T-type thermocouples and RTDs over an extended operational period, signals from the RTDs, T-type thermocouples, pressure transducers, flowmeters, and heaters were collected using a data acquisition system.

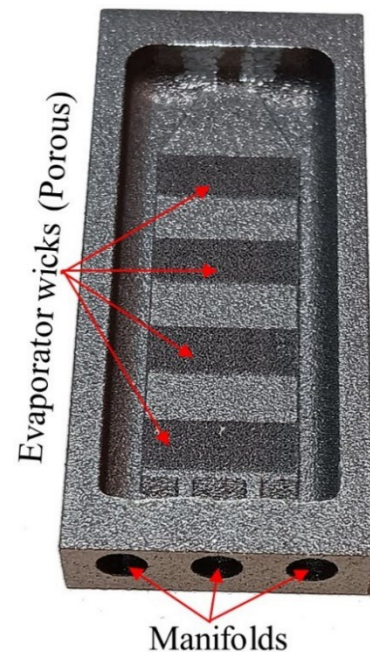


FIGURE 6: INTERIOR SECTION OF THE COLD PLATE REPRESENTING THE EVAPORATOR WICKS

TABLE 1: GEOMETRICAL INFORMATION OF THE COLD PLATE AND EVAPORATOR WICKS.

L_c, H_c, W_c	65.8 mm, 10.4 mm, 28.7 mm
L_p, W_p, d_p	3.8 mm, 3.0 mm, 11.2 mm
L_w, W_w, t_w	15.2 mm, 5.6 mm, 1.0 mm

The entire loop was covered with insulation layers to minimize the heat exchange with the surroundings. The heat loss from the cold plate was determined by performing a series of

single-phase tests and calculating the heat transfer ratio, i.e., ϕ , corresponding to the ratio of sensible heat absorbed by the refrigerant to the electrical heat input. Then, q_i , corresponding to the heat flux applied to the i -th pedestal was calculated as follows:

$$q_i = \phi \frac{V_i \times I_i}{L_p \times W_p} \quad (1)$$

where L_p and W_p represent the length and width of the pedestal where it is affixed to the cold plate, respectively, and specified in Fig. 2 and Table 1. Also, V_i and I_i are the voltage and current applied to the i -th heater, respectively. The thermal performance of the cold plate was evaluated by calculating the specific thermal resistance of each individual heater (R_i), representing the thermal resistance from the location of the thermocouple in the pedestal to the coolant, expressed as follows:

$$R_i = \frac{T_{s,i} - \left(\frac{T_{in} + T_{out}}{2} \right)}{q_i} \quad (2)$$

where $T_{s,i}$ represents the corresponding source temperature of the i -th heater, as measured by the thermocouple located in the i -th pedestal, as shown in Fig. 2. Also, T_{in} and T_{out} are the inlet and outlet temperatures of the refrigerant, respectively. These temperatures were measured using their respective RTDs at the inlet and outlet manifolds.

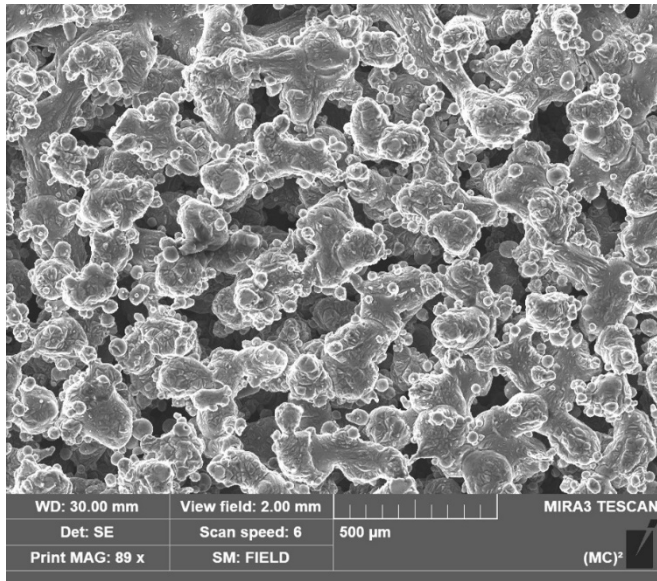


FIGURE 7: SEM IMAGE OF THE EVAPORATOR WICK

3. RESULTS AND DISCUSSION

The experiments were conducted by horizontally placing the cold plate inside the loop, with the arrangement of heaters following a sequence similar to the one shown in Fig. 3. The thermal resistances as functions of heat fluxes for the plain cold

plate and capillary-driven cold plate (i.e., HTPCS) are illustrated in Fig. 8 and Fig. 9, respectively. To facilitate more accurate comparisons, the axis scales of both graphs were maintained consistently. As the heat load increases, evaporation/boiling enhances, resulting in a reduction of thermal resistance. This trend persists until a global minimum thermal resistance is reached, indicating partial dryout. Partial dryout signifies a balance between the rate of liquid depletion due to evaporation/boiling and the rewetting capability of the evaporator. Beyond partial dryout, further increases in the heat load lead to an elevation in thermal resistance, expediting the onset of CHF. In this study, CHF was identified by a sharp increase in the corresponding temperature of any of the heaters.

The performance of the plain cold plate displayed variability concerning the top- and bottom-level heaters. To better comprehend the impact of this inconsistency on the overall cold plate performance, experiments testing the plain cold plate were extended until the identification of CHF for any of the eight heaters. Up to a heat flux of around 320 W/cm², the corresponding thermal resistances for all bottom-level heaters consistently decreased as the heat load increased, reaching values of approximately 0.17-0.20 K-cm²/W. However, partial dryout occurred at significantly lower heat fluxes for heaters 1, 2, and 4, around 140-147 W/cm². Continuing operation beyond the corresponding partial dryout of bottom-level heaters increased the risk of CHF occurring in the top-level heaters, eventually affecting the bottom-level heaters, with all heaters reaching CHF at approximately 320-350 W/cm². Therefore, the plain cold plate could operate at heat fluxes below 150 W/cm², with a wide range of measured thermal resistances ranging from 0.18 to 0.32 K-cm²/W.

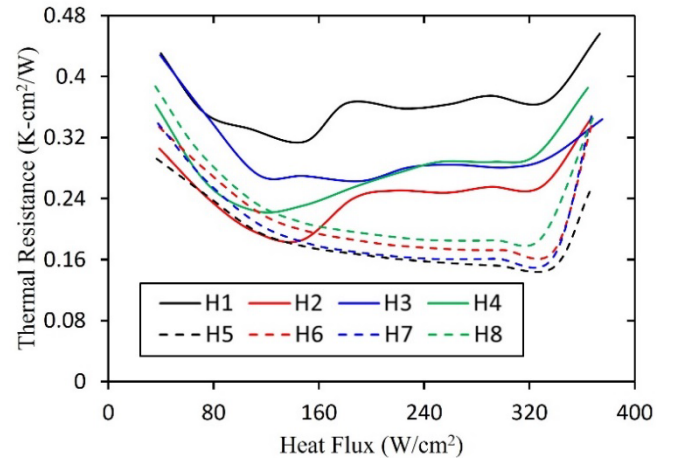


FIGURE 8: THERMAL RESISTANCE OF THE PLAIN COLD PLATE AT DIFFERENT HEAT FLUXES

The wick structures in the capillary-driven cold plate, owing to their porous nature, increase the number of nucleation sites and menisci, promoting boiling and evaporation, respectively. This leads to a lower thermal resistance when compared to the plain cold plate. Moreover, the capillary pressure generated by the wicks in the capillary-driven cold plate enhances the

evaporator's rewetting ability compared to the plain cold plate. Consequently, this contributes to an increased upper limit operation for the capillary-driven cold plate. As shown in Fig. 9, the capillary-driven cold plate (i.e., HTPCS) substantially improved the thermal performance of the plain cold plate. The thermal resistances of all heaters decreased as the heat load increased, reaching partial dryout on the corresponding evaporator of heater 7 at a heat flux of approximately 305 W/cm². However, beyond this point, other evaporators did not experience partial dryout. Eventually, all heaters reached CHF at heat fluxes around 345-350 W/cm². Therefore, the HTPCS demonstrated effective operation up to 305 W/cm², exhibiting measured thermal resistances ranging from approximately 0.17 to 0.24 K-cm²/W. Utilizing the evaporator wicks, the capillary-driven cold plate enhanced the upper limit operation of the plain cold plate by more than 103%.

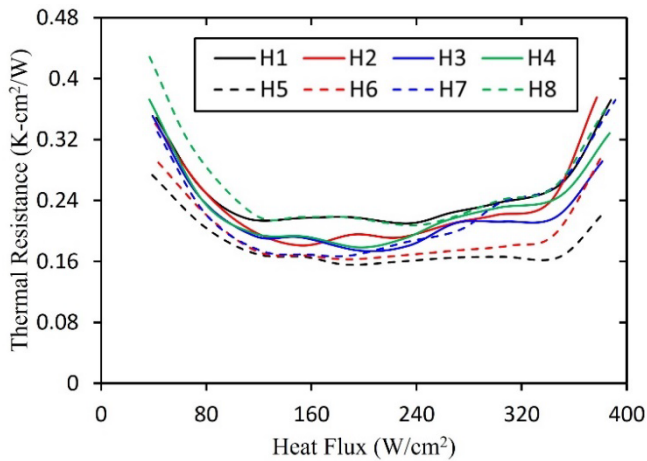


FIGURE 9: THERMAL RESISTANCE OF THE CAPILLARY-DRIVEN COLD PLATE (i.e., HTPCS) AT DIFFERENT HEAT FLUXES

Operating with low pumping power is an important characteristic of an efficient active cooling system, as excessive pumping power can hinder the practical implementation of the cooling technology, even if it exhibits high thermal performance [21,22]. The pumping power is determined by multiplying the volume flow rate with the pressure drop across the entire system. Through the utilization of appropriately sized transport tubes, it was possible to minimize the pressure drop experienced within the pumped two-phase loop. Consequently, the primary pressure drop within the system takes place across the cold plate. This pressure drop was calculated by deducting the outlet pressure from the inlet pressure, utilizing the pressure measurements acquired from their respective pressure transducers. One of the notable aspects of a HTPCS is its capability to operate with a low flow rate that is only adequate for supplying the liquid to the evaporator wicks for evaporation. In the present study, the HTPCS operated with a low pumping power below 0.08 W.

In this study, the developed HTPCS integrated with 3D printed capillary-driven cold plate showcased remarkable attributes, including consistently low thermal resistances, highly

uniform thermal resistance across the cold plate, and operating with low pumping power. Moreover, the entire cold plate was fabricated through one single 3D printing process, resulting in significant cost and time savings compared to conventional cold plate manufacturing methods used in existing HTPCSs. These collective advantages position the developed HTPCS, featuring the 3D printed cold plate, as an appealing cooling technology for applications involving high-heat-flux electronics.

4. CONCLUSION

In this study, a HTPCS integrated with a 3D printed cold plate made of AlSi10Mg was developed. The cold plate was fabricated using one single 3D printing process, significantly reducing both cost and time compared to manufacturing current versions of cold plates used in HTPCSs. The developed HTPCS operated at heat fluxes exceeding 305 W/cm² and achieved uniform thermal resistances across the cold plate, as low as 0.17 to 0.24 K-cm²/W, while operating with a low pumping power below 0.08 W. The HTPCS enhanced the upper limit operation of the plain cold plate by more than 103%. The high thermal performance of the HTPCS, combined with its substantially simplified fabrication process through one single 3D printing process, positions the developed HTPCS in this study as an attractive thermal management solution for the next generation of high-heat-flux electronics.

ACKNOWLEDGEMENTS

Financial support by the Office of Science in the U.S. Department of Energy, award number DE-SC0018845 is gratefully acknowledged. Also, the authors appreciate Dr. Massoud Kaviani from the Department of Mechanical Engineering at the University of Michigan, Ann Arbor, for providing the SEM image of the 3D printed wicks.

REFERENCES

- [1] Wang H J, Xu J Y and Hong F J 2022 Developing of an open-source toolbox for liquid-vapor phase change in the porous wick of a LHP evaporator based on OpenFOAM *Case Stud. Therm. Eng.* **35** 102068
- [2] Shaeri M R, Attinger D and Bonner R W 2018 Vapor chambers with hydrophobic and biphilic evaporators in moderate to high heat flux applications *Appl. Therm. Eng.* **130** 83–92
- [3] Shaeri M R, Chen C-H, Bonner R W and Demydovych M 2023 Demonstration of CTE-Matched Two-Phase Minichannel Heat Sink 2023 22nd IEEE Intersociety Conference on Thermal and Thermomechanical Phenomena in Electronic Systems (ITherm) (Orlando, FL, USA: IEEE) pp 1–5
- [4] Dede E M, Zhang C, Wu Q, Seyedhassantehrani N, Shattique M, Roy S, Palko J W, Narumanchi S, Kekelia B, Hazra S, Goodson K E, Giglio R and Asheghi M 2023

- Techno-economic feasibility analysis of an extreme heat flux micro-cooler *iScience* **26** 105812
- [5] Ma X, Ji X, Wang J, Yang X, Zhang Y and Wei J 2022 Flow boiling instability and pressure drop characteristics based on micro-pin-finned surfaces in a microchannel heat sink *Int. J. Heat Mass Transf.* **195** 123168
- [6] Lee M and Park C 2022 Mechanical-capillary-driven two-phase loop: Feedback control for thin-film evaporation and capillary limit enhancement *Appl. Therm. Eng.* **204** 117960
- [7] Lee M and Park C 2018 Mechanical-capillary-driven two-phase loop: Numerical modeling and experimental validation *Int. J. Heat Mass Transf.* **125** 972–82
- [8] Wrobel R and McGlen R J 2021 Heat pipes in thermal management of electrical machines – A review *Therm. Sci. Eng. Prog.* **26** 101053
- [9] O’Neill L E and Mudawar I 2020 Review of two-phase flow instabilities in macro- and micro-channel systems *Int. J. Heat Mass Transf.* **157** 119738
- [10] Lee S, Devahdhanush V S and Mudawar I 2019 Experimental and analytical investigation of flow loop induced instabilities in micro-channel heat sinks *Int. J. Heat Mass Transf.* **140** 303–30
- [11] Shaeri M R, Bonner R W and Ellis M C 2020 Thin hybrid capillary two-phase cooling system *Int. Commun. Heat Mass Transf.* **112** 104490
- [12] Wang Z, Chen C, Millet D and Zhang Y 2023 Parametric Scaffold Design for Property Control of Multi-Material Structure in Metallic Hybrid Additive Manufacturing *Procedia CIRP* **119** 241–7
- [13] Roux L L, Liu C, Ji Z, Kerfriden P, Gage D, Feyer F, Körner C and Bigot S 2021 Automatised quality assessment in additive layer manufacturing using layer-by-layer surface measurements and deep learning *Procedia CIRP* **99** 342–7
- [14] dos Santos Paes L E, Ferreira H S, Pereira M, Xavier F A, Weingaertner W L and Vilarinho L O 2021 Modeling layer geometry in directed energy deposition with laser for additive manufacturing *Surf. Coat. Technol.* **409** 126897
- [15] Tofail S A M, Koumoulos E P, Bandyopadhyay A, Bose S, O’Donoghue L and Charitidis C 2018 Additive manufacturing: scientific and technological challenges, market uptake and opportunities *Mater. Today* **21** 22–37
- [16] Kaur I and Singh P 2021 State-of-the-art in heat exchanger additive manufacturing *Int. J. Heat Mass Transf.* **178** 121600
- [17] Shaeri M R, Bonner R and Catuche J 2023 Additively Manufactured Hybrid Two-Phase Cold Plate *ASME 2023 International Technical Conference and Exhibition on Packaging and Integration of Electronic and Photonic Microsystems* ASME 2023 International Technical Conference and Exhibition on Packaging and Integration of Electronic and Photonic Microsystems (San Diego, California, USA: American Society of Mechanical Engineers) p V001T07A001
- [18] Catuche J, Shaeri M R and Ellis M C 2022 Additive Manufacturing of Capillary-Driven Two-Phase Cold Plates *Proceedings of the 8th World Congress on Mechanical, Chemical, and Material Engineering (MCM’22)* (Czech Republic, Prague) p HTFF 174
- [19] Shaeri M R, Attinger D and Bonner R 2017 Feasibility study of a vapor chamber with a hydrophobic evaporator substrate in high heat flux applications *Int. Commun. Heat Mass Transf.* **86** 199–205
- [20] Ju Y S, Kaviany M, Nam Y, Sharratt S, Hwang G S, Catton I, Fleming E and Dussinger P 2013 Planar vapor chamber with hybrid evaporator wicks for the thermal management of high-heat-flux and high-power optoelectronic devices *Int. J. Heat Mass Transf.* **60** 163–9
- [21] Shaeri M R and Bonner R W 2018 Lightweight and high-performance air-cooled heat sinks *2018 34th Thermal Measurement, Modeling & Management Symposium (SEMI-THERM)* 2018 34th Thermal Measurement, Modeling & Management Symposium (SEMI-THERM) (San Jose, CA: IEEE) pp 224–7
- [22] Shaeri M R and Bonner R 2019 ADVANCES IN LIGHTWEIGHT HEAT SINKS *Proceeding of 4th Thermal and Fluids Engineering Conference* 4th Thermal and Fluids Engineering Conference (Las Vegas, NV, USA: Begellhouse) pp 839–42